ZURICH, SWITZERLAND
6 - 10 OCTOBER 2025

EUROPEAN GEOTHERMAL CONGRESS 2025

Numerical simulation of a single-well closed-loop deep borehole heat exchanger (DBHE) at the Groß Schönebeck site

Lingkan Finna Christi[1,2], Mrityunjay Singh[1,3], Maximilian Frick[1], Hannes Hofmann[1,2], Ben Norden[1], Ingo Sass[1,3]

[1] GFZ Helmholtz Center for Geosciences, Telegrafenberg, 14473 Potsdam, Germany
[2] Technische Universität Berlin, Straße des 17. Juni 135, 10623 Berlin, Germany
[3]Technische Universität Darmstadt, Schnittspahnstraße 9, 64287 Darmstadt, Germany

Keywords: Groß Schönebeck, North German Basin, single-well closed-loop, deep borehole heat exchanger (DBHE), repurposing hydrocarbon well, deep geothermal.

ABSTRACT

The Groß Schönebeck site, located in the North German Basin, has served as a demonstration platform for the conversion of a 4.3 km deep gas exploration well, E GrSk 3/90, into a geothermal research well since 2000. In 2006, a new geothermal well was drilled to a depth of 4.4 km with the intention of serving as a geothermal production well. Subsequently, a multidisciplinary research platform was developed at the Groß Schönebeck site to demonstrate the extraction of geothermal energy using a well doublet. The aim of this study is to numerically simulate the application of a single-well closed-loop deep borehole heat exchanger (DBHE) in the existing wells E GrSk 3/90 and Gt GrSk 4/05 (A2). The model was constructed using the latest 3D geological model of the Groß Schönebeck site, which was derived from the 3D seismic interpretation carried out in 2017. The DBHE is set at a depth of 3800 m true vertical depth (TVD) with a temperature of 138 ℃ in both E GrSk 3/90 and Gt GrSk 4/05 (A2) wells as an alternative way to use the existing wells. At this depth, the maximum casing diameter of each well is 7”, and the wells penetrate the Straßfurt Formation of the Permian Zechstein. The numerical simulation of the coaxial DBHE at the Groß Schönebeck site shows that with a maximum bottom hole temperature of 138 ℃, an inlet temperature range between 10 ℃ and 20 ℃, and a maximum flow rate of 54.00 m^3h^{-1}, a maximum thermal power of 1000 kW can be achieved by the two deep wells.

1. INTRODUCTION

The discovery of the gas exploration well E GrSk 3/90 well, a gas exploration well, led to the development of the Groß Schönebeck geothermal research platform, as shown in Figure 1. The well was originally drilled in 1990 to target a Rotliegend gas reservoir at a depth of more than 4 km. However, the well was closed immediately after drilling due to the presence of insufficient gas deposits. A decade later, in 2000, the well was identified as a potential candidate for reuse as a geothermal research well, and was selected from 50 abandoned oil and gas exploration wells in Northeastern Germany that had been plugged and abandoned (Huenges et al., 2002).The selection was predicated on the observed bottom-hole temperature of 149 ℃ at 4240 m True Vertical Depth (TVD) and the substantial regional extent of the Rotliegend formation as a potential geothermal reservoir (Huenges et al., 2002). At the Groß Schönebeck site, the anticipated reservoir target of the Rotliegend sediments and volcanics manifested inadequate permeability to facilitate the delivery of geothermal fluids. As a result, since 2001, the site has been designated as a demonstration site, focusing on the development of matrix-dominated EGS concept.

The second well dedicated to geothermal production, Gt GrSk 4/05 (A2), was drilled in 2006 (Huenges et al., 2007). The chronology of the site development as an EGS doublet well from 2001 to 2013, and the subsequent hydraulic fracturing, have been summarized in the studies of Blöcher et al. (2016) and Christi et al. (2025). During series of hydraulic tests between E GrSk 3/90 and Gt GrSk 4/05 (A2), a severe drop in productivity was observed between 2011 and 2013. The factors that may have contributed to the observed decline in productivity during these tests have been discussed in Blöcher et al. (2016) and investigated by Regenspurg et al. (2015, 2016). These studies placed particular emphasis on the issues of clogging and corrosion in the production liner of Gt GrSk 4/05 (A2). This issue is proving to be a major obstacle to progressing the matrix-dominated EGS development concept at Groß Schönebeck. A slug withdrawal test measurement conducted in 2021 (Regenspurg et al., 2024) revealed that the productivity index (PI) of 0.6 $m^3\ h^{-1}\ MPa^{-1}$ has remained constant over the past decade. This is notable given that during this period the well has not been pumped, with the exception of small volumes utilized for testing and sampling purposes. The objective of this study is to evaluate the viability of repurposing the infrastructure at the Groß Schönebeck site to promote the application of a coaxial deep borehole exchanger technology as an alternative option to further develop the Groß Schönebeck site.

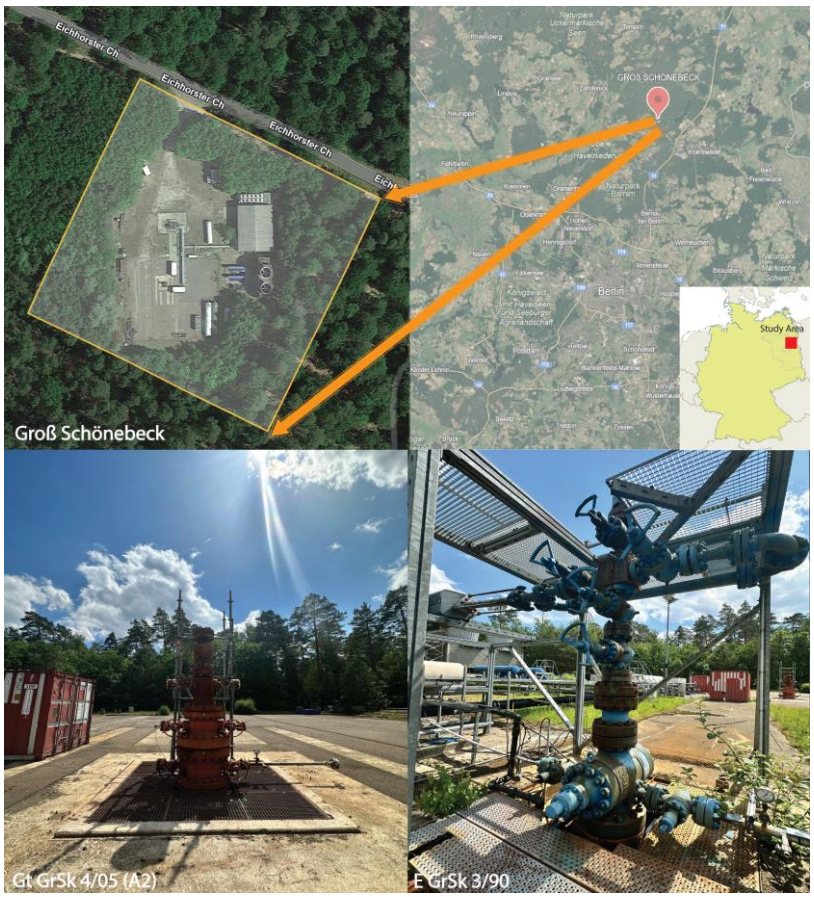

Figure 1: Location of the Groß Schönebeck site.

The coaxial DBHE technology has already been implemented in Prenzlau (Schneider et al., 1997) and Landau (LBEG, 2021). Both are the two sites where the first three BHE technologies were installed in Germany.

2. GEOTHERMAL POTENTIAL OF THE GROß SCHÖNEBECK SITE

The study evaluated geothermal potential based on temperature gradient and formations intersected by the wells, especially those suitable for coaxial closed-loop technology. As reported in Huenges et al. (2002), five temperature logs were obtained following the reopening of E GrSk 3/90, with measurements conducted over a period of nine months. The mean temperature at the bottom increased by approximately 0.5 ℃, while in the shallow part of the first 1500 m TVD, it decreased by 2 ℃. This phenomenon was found to be associated with differing thermal conductivities across different lithology. The Zechstein section, characterized by its notably high thermal conductivity, exhibited minimal temporal variations. Consequently, it can be concluded that heat transport in this formation occurred predominantly by conduction.

The Zechstein Formation consists of cyclic evaporite deposits, with the 4.3 and 4.4 km (measured depth) doublet wells at the Groß Schönebeck site comprising approximately 1500 m of this formation. The presence of salt structures, as described in Huenges et al. (2002) and Norden et al. (2023), strongly influences the subsurface temperature field at the Groß Schönebeck site. The phenomenon exhibits elevated thermal conductivities in the Zechstein formation compared to the overlying sedimentary sequences, thereby inducing substantial small-scale thermal anomalies, a phenomenon referred to as the "chimney effect" (Fromme et al., 2010; Noack et al., 2010; Kaiser et al., 2011; Balling et al., 2013; Sippel et al., 2013; Koltzer et al., 2024). Consequently, the augmented temperature potential in the upper portion of salt structures can be harnessed with closed systems, such as near-surface, intermediate depth, or deep borehole heat exchangers (Fromme et al., 2010). In a hydrocarbon system, salt is a tight and sealing lithology, which is the most ideal caprock for a hydrocarbon system (Grunau, 1981; Jin et al., 2006; Liu et al., 2017). Therefore, in the hydrocarbon system, salt contribute to the formation's significantly low permeability, which is close to zero.

3. METHODOLOGY

In this study, numerical model of a coaxial DBHE system was then carried out to assess the geothermal potential at the maximum depth of 3800 m TVD which is the base of the Zechstein Formation with a maximum temperature of 138 ℃ and a permeability of 9.87×10^{-20} m^2. The optimum diameter of the well configuration is critical to maximizing energy recovery. The configuration of the well has been demonstrated to exert a significant influence on the depth and dimensions of the coaxial tubing, as well as the most accessible temperature within the borehole. The bottom-hole casing diameter at the respective depths of

both wells is 7 inches. This is to allow for the maximum diameter of the coaxial tubing installation scenario. The variation in thermal conductivity of each formation is based on the work of Norden et al. (2008, 2012, 2023) and Blöcher et al. (2010), where the thermal conductivity of the Zechstein formation ranges from 3.5 to 5.4 W m^{-1} K.

A numerical model of the coaxial DBHE system was developed and evaluated using CMG STARS, a commercial finite-difference reservoir simulator capable of representing coupled thermal and hydraulic dynamics in geothermal reservoirs. The complete wellbore is simulated with Flexwell, which applies an independent flow and heat transfer models integrated with the reservoir model. In each simulation time step, the process first resolves the wellbore model while maintaining a constant reservoir state. Subsequently, the reservoir state is updated while holding the wellbore conditions fixed. This sequential approach results in the reservoir calculations lagging one iteration behind the wellbore. The combined reservoir and wellbore framework is developed by using energy conservation, incorporating mass and momentum balances. Both laminar and turbulent flow regimes along the pipe, as well as the effects of pipe roughness, are taken into account. Moreover, heat loss is modeled via conductive heat transfer between the tubing and the annulus and from the annulus to the reservoir, with the overall heat transfer coefficient is determined by the cumulative thermal resistance of the tubing, annular space, and reservoir blocks.

3.1 Model setup

The geometry of the reservoir model was defined on the basis of the 3D geological model based on the latest 3D seismic interpretation of the Groß Schönebeck site (Norden et al., 2023). Fifteen geological units intersected by the well doublet are represented in the 3D model with dimensions of 0.45 km (x/i) × 0.32 km (y/j) × 4.5 km (z/k). Each individual grid cell has a dimension (Δx, Δy) of 10 m x 10 m, with the vertical length (Δz) varying according to the thickness of the defined geological unit as described in Table 1. For coaxial DBHE modeling, the interaction between the wellbore and the reservoir is limited to the near-wellbore area, therefore the grid was designed to cover the area of the trajectory with a 50 m margin on either side of the reservoir grid.

The grid was discretized with a discretization factor of 5 (x/i) × 5 (y/j) × 5 (z/k) within the area intersected by both wells as shown in Figure 2 (A, B, C). The well completions, as described by Christi et al. (2025), were implemented accordingly for wellbore models of E GrSk 3/90 Gt GrSk 4/05 (A2).

3.2 Model parameterization

The model parameterization is classified according to the main aspects of modeling a closed-loop system. These are boundaries and initial conditions, reservoir and wellbore parameters, and working fluid as detailed in Table 1.

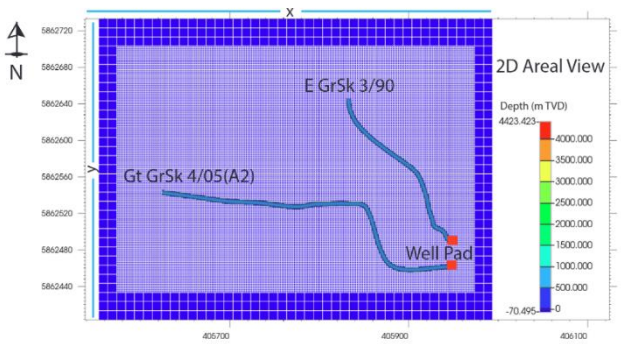

(A)

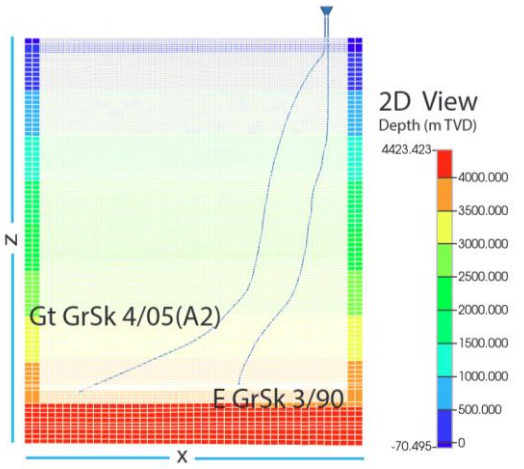

(B)

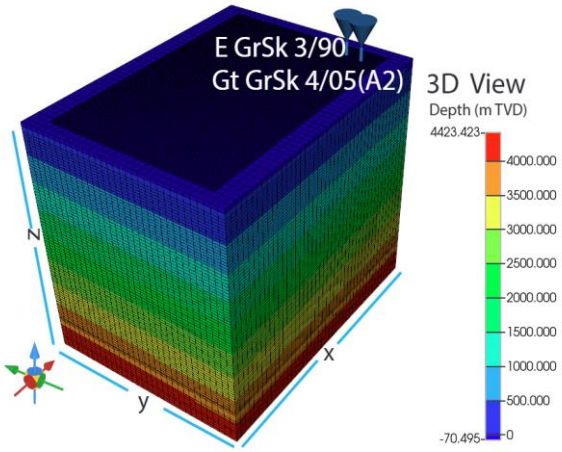

(C)

Figure 2: (A) 2 D Areal view of model setup (i,j direction); (B) 2D Areal view of model setup (i,k direction); (C) 3D view of the model setup (i, j, k directions).

Table 1: Model parameterization.

1. Boundary and Initial conditions					
Parameter	Symbol	Unit			
Initial condition					
Surface temperature	T	℃	10.00		
Temperature gradient	∇T	℃ m^{-1}	(IEA,2022) 0.032		
Pressure at 4290 m TVD	p	MPa	45.5		
2. Working Fluid					
Parameter	Symbol	Unit			
Water thermal conductivity	λ_f	$Wm^{-1}K^{-1}$	0.6065 (Ramires et al., 1995)		
Water density	ρ_w	kg m^{-3}	(Younglove and Ely, 1987)		
Viscosity	μ_w	mPa s	(Schmelzer et al., 2005)		
Liquid compressibility	CP_{Water}	kPa^{-1}	4.7×10^{-7}		
Specific heat capacity	C_{pw}	MJ $m^{-3}K^{-1}$	4.19		
3. Reservoir Property					
Parameter	Symbol	Unit			
Porosity of Zechstein Formation	ϕ	-	0.05		
Permeability of Zechstein Formation	k	m^2	9.87×10^{-20}		
Formation Compressibility	CP_{rock}	kPa^{-1}	4.50×10^{-7}		
Formation	Rock Thermal Conductivity (λ_r), ($Wm^{-1}K^{-1}$)		Rock Heat Capacity (C_{pr}), ($MJm^{-3}K^{-1}$)	Thickness (m)	Spatial model layers
Surface - Tertiary	2.38		1.65	168	3
Cretaceous	2.82		2.29	165	2
Lias	2.53		2.53	315	6
Keuper	2.71		2.32	593	11
Muschelkalk	2.30		2.25	309	6
Bundsandstein	2.27		2.32	819	16
Zechstein (Staßfurt - Werra Fm.)	4.50		2.32	1498	29
Rotliegend (Hannover Fm.)	1.90		2.40	208	3
Rotliegend (Dethlingen Fm.)	2.80		2.40	100	2
Rotliegend (Havel Fm.)	3.00		2.60	38	1
Rotliegend (Effusive Rotliegend)	2.30		3.60	70	2
Permo-Carboniferous Volcanic	2.30		3.60	217	4
4. Wellbore Property					
Component	Thermal Conductivity (λ_r), ($Wm^{-1}K^{-1}$)		Heat Capacity (C_{pr}), ($MJm^{-3}K^{-1}$)	Outer Diameter (inch)	Inner Diameter (inch)
Cement	1.37		1.85	8.75-17.75	9.63 – 18.63
Casing - Carbon Steel	45.00		3.82	7.00 – 16.00	6.00 – 14.85
Tubing - Carbon Steel	45.00		3.82	2.88	2.44
Insulator	0.19		0.003	Thickness: 1.215	

The boundary conditions encompass the defined temperature and pressure for the bottom and top boundaries. The initial temperature of the reservoir model is calculated based on an average temperature gradient of the Rotliegend formation, which is specified as 0.032 ℃ m^{-1} using equation 1. The initial hydrostatic pressure was determined using equation 2. The pressure of the entire block was calculated using the vertical equilibrium, depth-averaged capillary gravity method without considering a phase pressure correction. Constant pressure and temperature boundary conditions

are applied to the sides of the model by assuming an infinite reservoir.

$$\nabla T = 0.032\ ℃\ m^{-1} \times depth\ (m\ TVD) + 10℃ \quad (1)$$

$$p = \rho\ g\ z \quad (2)$$

The initial pressure was calculated based on Equation 2 with a reference reservoir fluid density (ρ) of 1150 kg m^{-3}, a gravity acceleration (g) of 9.80 m s^{-2}, and a water column height (z) of 4035 m based on the measurement of average water level of 255 m from the well bottom-hole of 4290 m TVD. Water is used as a working fluid. Petrothermal properties of the reservoir such as rock thermal conductivity (λ_r) and rock specific heat capacity (C_{pr}) were applied to the model and they are listed in Table 1. These two parameters are the critical parameters for feasibility analysis. As for the closed-loop system, permeability and porosity are set based on the properties of the Zechstein formation.

Wellbore parameters such as borehole length and casing diameter are set as describe in Table 1. Thermal conductivity (λ_l) and heat capacity (C_{pl}) were set for the annulus, tubing, insulators, and cement based on the materials.

3.3 Operating condition parameters

The first consideration is the flow rate used in the design process to determine the optimum flow rate and injection capacity for the well. It is imperative to consider both the maximum allowable bottom hole pressure at 3800 m TVD and the pressure along the wellbore when determining the flow rate. In this study, simulations were performed at the following flow rates: 3.60 m^3h^{-1}, 18.00 m^3h^{-1}, 36.00 m^3h^{-1}, and 54.00 m^3h^{-1}. The pressure constraint was set at 55 MPa to prevent the injection pressure from exceeding the minimum horizontal stress (Shmin). The temperature ranges of 10℃, 25℃, 30℃, 40℃, 50℃, 60℃, 70℃, and 80℃ were assigned in the simulation scenarios. The calculation of thermal power P [W] for each scenario was performed according to the equation 3.

$$P = \rho_f c_f Q\ (T_0 - T_i) \quad (3)$$

Using the pressure and the temperature dependent specific heat capacity (c_{pw}) [MJ m^{-3}K)] and density (ρ_w) [kg m^{-3}], as well as inlet temperature (T_i) [°C] as input parameters, and the outlet temperature (T_o) [°C] resulting from the simulations.

4. RESULTS

The results are presented to evaluate (1) the maximum circulated flow rate to the DBHE system by evaluating the bottom-hole pressure at a depth of 3800 m TVD at a given flow rate, (2) the wellbore pressure along the tubing, (3) the range of inlet and outlet temperatures, (4) the reservoir temperature decline at a depth of 3800 m TVD over the 30-year simulation scenario, (5) the generated thermal power of different combinations of operating parameters.

4.1 Bottom-hole pressure vs flow rate

At the base case inlet temperature of 10℃, the bottom-hole pressures at the given constant flow rates of 3.60 m^3h^{-1}, 18.00 m^3h^{-1}, 36.00 m^3h^{-1}, and 54.00 m^3h^{-1} are shown in Figure 3. The bottom-hole pressures are given assuming that the perforation at the bottom-hole of 3800 m TVD is exposed to the impermeable reservoir, the Zechstein formation. This information provides a constraint on the maximum allowable flow rate given to the closed-loop system.

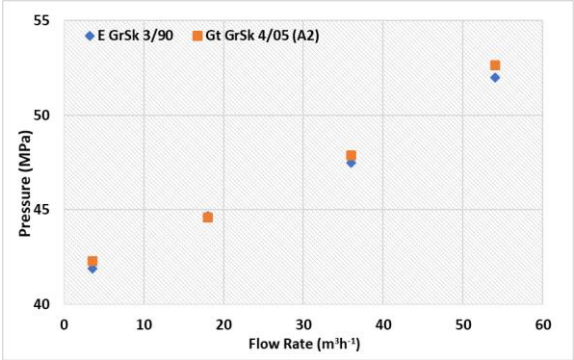

Figure 3: Well bottom-hole pressure at a depth of 3800 m TVD for different flow rates.

4.2 Wellbore pressure profiles

The wellbore pressure in the annulus at the first time-step of the transient state in the simulation is shown in Figure 4, for wells E GrSk 3/90 and Gt GrSk 4/05 (A2).

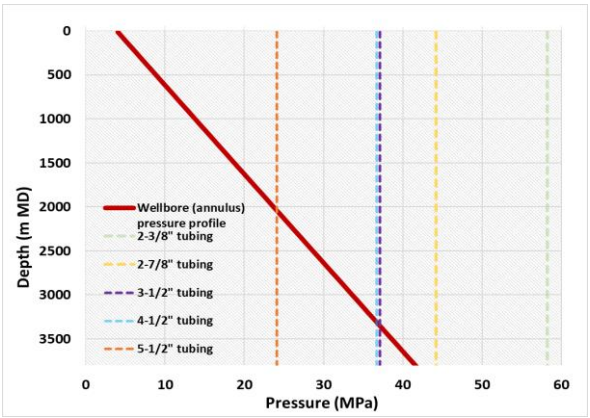

Figure 4: Wellbore pressure profile at E GrSk 3/90 and Gt GrSk 4/05.

The graph shows the annulus pressure profile. The wellbore pressure remains constant at the initial inlet temperature of 10 °C and at various given flow rates of 3.60 m^3h^{-1}, 18.00 m^3h^{-1}, 36.00 m^3h^{-1}, and 54.00 m^3h^{-1}. As the flow rate increases, there is no additional pressure increase along the wellbore annulus. When designing a closed-loop coaxial system, the annulus pressure is important in determining the depth at which the coaxial tubing should be installed for a given maximum tubing pressure, corresponding to the tubing size. The maximum tubing pressure parameters are based on the commercially available tubing insulator.

4.3 Wellbore temperature profiles

The temperature profiles of both E GrSk 3/90 and Gt GrSk 4/05 (A2) in the 30th year of simulation at different flow rate scenarios and at the base case inlet temperature of 10℃ are shown in Figure 5 (A) and Figure 5 (B).

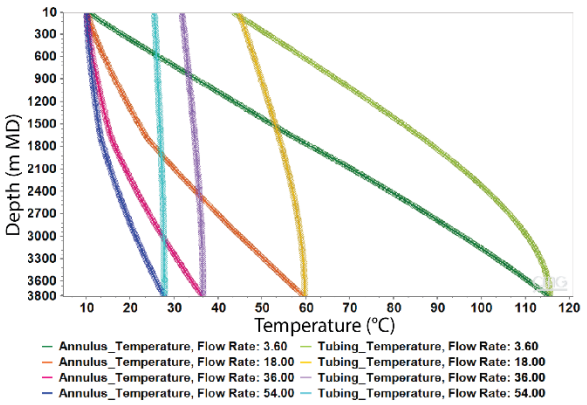

(A)

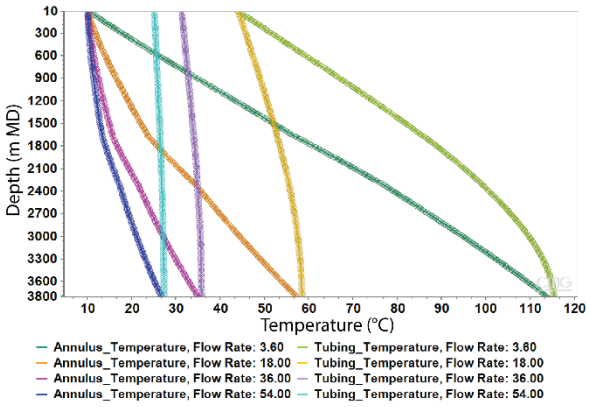

(B)

Figure 5: Annulus and tubing temperature profiles of (A) E GrSk 3/90; (B) Gt GrSk 4/05 (A2). Flow rate in m^3h^{-1}.

From the above figures, it can be seen that increasing the flow rate results in a decrease in the temperatures as shown by the annulus and tubing temperature profiles of both wells. The flow rate has a direct effect on the temperature along the wellbore. The maximum temperature differences are shown at a flow rate of 18 m^3h^{-1}. At the lowest flow rate of 3.60 m^3h^{-1}, the temperature of the injected water can reach 115 ℃ at the bottom of the well, while the injected temperature is 10 ℃.

4.4 Outlet temperature and reservoir temperature decline

The tubing outlet temperature over the 30-year simulation scenario at different flow rate scenarios at a constant temperature of 10℃ is shown in Figure 6 (A) for both wells E GrSk 3/90 Gt GrSk 4/05 (A2). The reservoir temperature decline at the bottom-hole of both wells over the 30-year simulation scenario at the is shown in Figure 6 (B).

The two figures show that the continued decline in reservoir temperature does not affect the tubing outlet temperature of the coaxial DBHE system. Instead, the operating flow rates have a significant effect on the reservoir temperature drop and the outlet temperature. The higher the flow rate, the reservoir temperature decline increases.

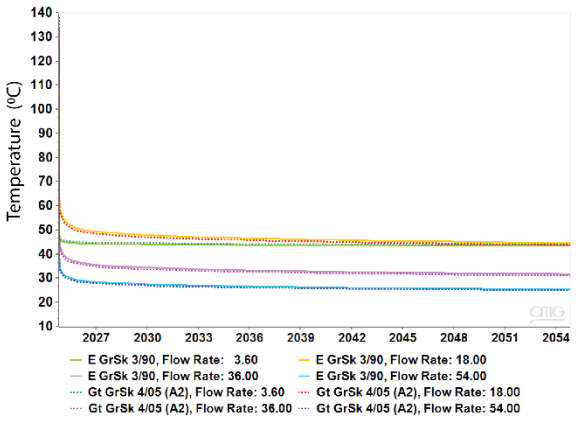

(A)

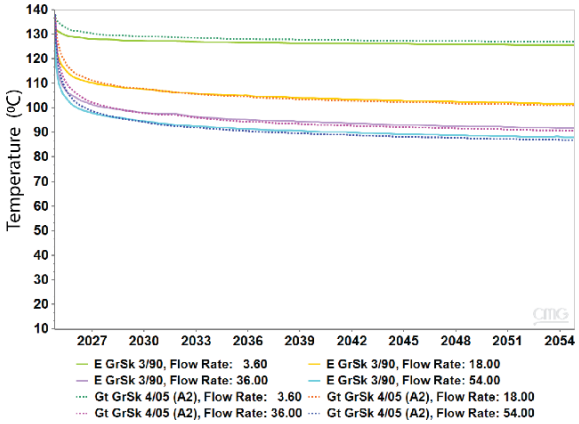

(B)

Figure 6: (A)Tubing outlet temperature; (B) Reservoir temperature at the bottom-hole (3800 m TVD) of both wells. Flow rate in m^3h^{-1}.

The decrease in outlet and reservoir temperature over time was also evaluated for given inlet temperatures at a constant flow rate of 18 m^3h^{-1}, as shown in Figure 7 and Figure 8 respectively. This is also to show how much the temperature drop depends on the inlet temperature.

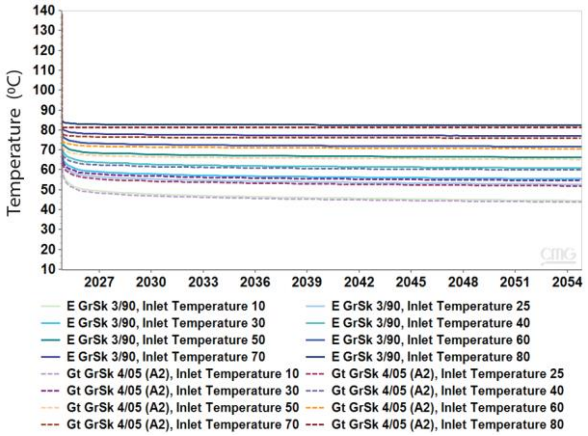

Figure 7: Outlet temperature at various given inlet temperatures.

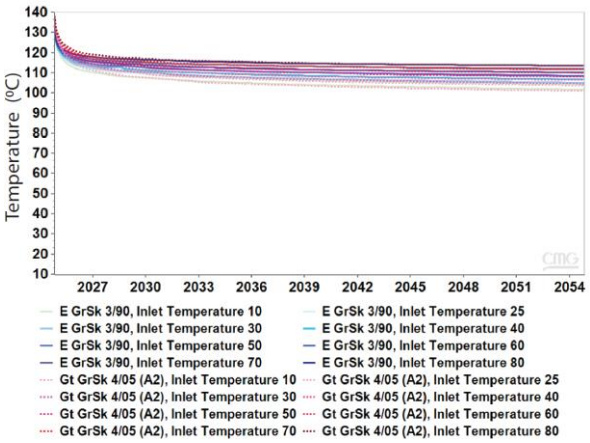

Figure 8: Reservoir temperature decline at various given inlet temperatures at a depth of 3800 m TVD.

As shown in both Figures 7 and 8, the outlet temperature and the bottom-hole reservoir temperature of both wells are directly affected by the given inlet temperature. The higher the temperature, the higher the outlet temperature, but the lower the reservoir temperature drop. At a constant flow rate of 18 m^3h^{-1}, with the range of inlet temperature of 10℃ to 80℃, the outlet temperature could reach a minimum of 44 ℃ and 82 ℃ at the maximum for 30-year simulation time. the reservoir temperature drop is around 37℃ from the initial temperature of 138 ℃ over the 30-year simulation time. The higher temperature does not result in the optimum heat gain of the fluid returning to the surface This will be explained by the relationship between the operating flow rate and the given inlet temperature to the coaxial closed-loop system.

4.5 Generated thermal power

The final results of thermal power generation from a combination of operating parameters for a 30-year simulation period are shown in Figure 9. These parameters include flow rate and inlet temperature with corresponding thermal power (kW). As shown in Figure 9, the optimum thermal power is obtained when the given inlet temperature is in the range of 1℃ to 20℃. In this inlet temperature range, the higher the flow rate, the higher the resulting thermal power. As indicated by the contour lines of the generated thermal power, a maximum of ~1000 kW of thermal power can be achieved at a flow rate range of 36.00 m^3h^{-1} to 54.00 m^3h^{-1} with an inlet temperature of less than 20℃. However, as the inlet temperature increases, the resulting thermal power decreases.

The optimum thermal power at the most stable flow rate of 18 m^3h^{-1} is approximately 700 kW with 10 ℃ inlet temperature. At this constant flow rate over a simulation period of 30 years, the resulting thermal power of both E GrSk 3/90 and Gt GrSk 4/05 (A2) are shown in Figure 10.

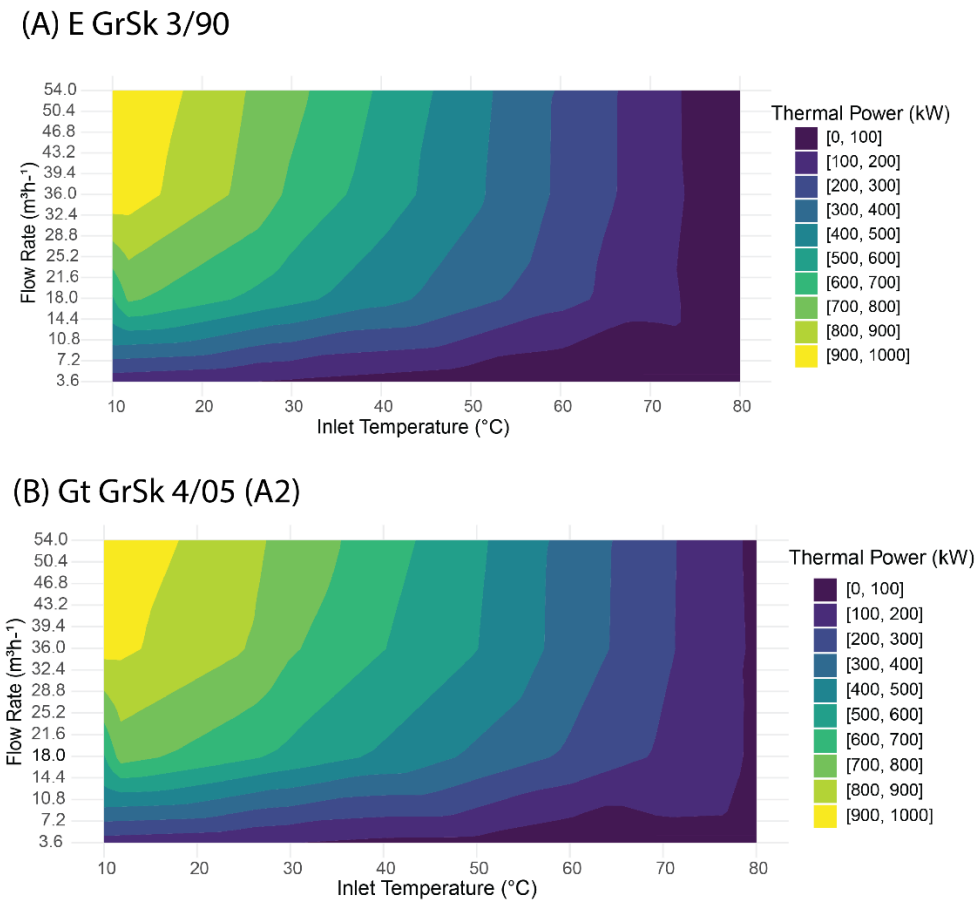

Figure 9: Thermal power (kW) produced at (A) E GrSk 3/90 and (B) Gt GrSk 4/05.

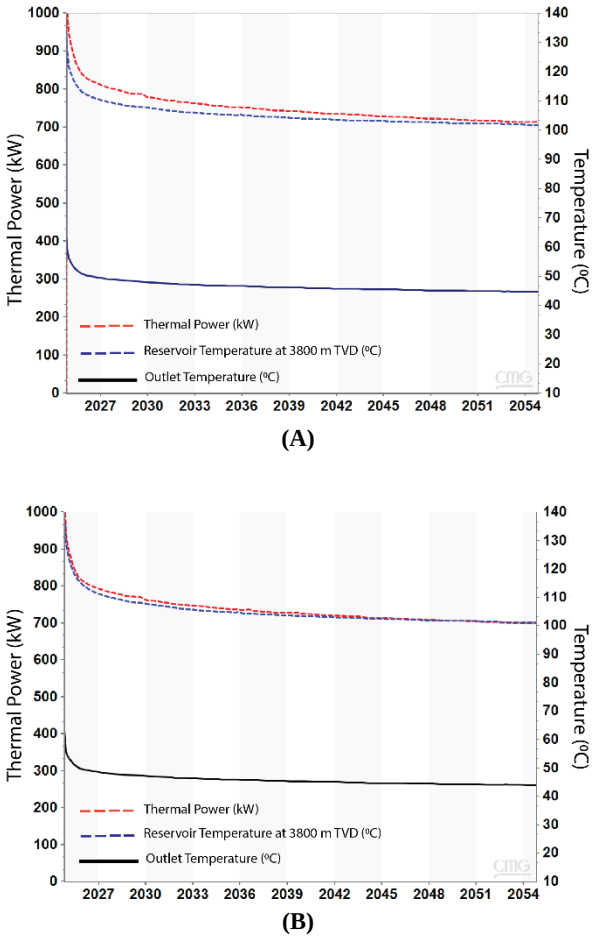

Figure 10: The optimum thermal power generated for the base case at 18 m^3h^{-1} flow rate and 10 °C inlet temperature for (A) E GrSk 3/90; (B) Gt GrSk 4/05 (A2).

5. DISCUSSION

In the context of the specified well configuration case study, the use of 2.44-inch inner tubing will result in a maximum wellbore pressure of 42 MPa and 43 MPa for E GrSk 3/90 and Gt GrSk 4/05 respectively, as shown in Figure 4 (A) and 4 (B). It is important to note that any increase of flow rate does not affect borehole pressure.

However, it should be noted that increasing the flow rate will result in a decrease in the number of heat transfer along the wellbore, as evidenced by the temperature profiles at both wells in Figures 5 (A) and 5 (B). The flow rate directly impacts the outlet temperature. The maximum outlet temperature difference ($T_0 - T_i$) is indicated at flow rate of 18 m^3h^{-1}. Even though, at the lowest flow rate of 3.60 m^3h^{-1}, the temperature of the injected water can reach 115 ℃ at the bottom-hole (3800 m TVD) while the inlet temperature is 10 ℃, the resulting outlet temperature of flow rate 18 m^3h^{-1} is the highest, as indicated by Figure 6(A).

A base-load scenario was simulated without a cyclic period of thermal power generation. It was assumed that the system would be circulated for the 30-year lifetime using different combinations of inlet temperatures and flow rates. The study evaluated the effect of continuous injection on reservoir temperature stability, focusing particularly on the reservoir temperature at a depth of 3800 m TVD, surrounding the bottom-hole well. As shown in Figure 6 (B), an increase in flow rate is associated with an increase in the reservoir temperature decline of both wells. While the decrease is less pronounced at minimum flow rates, a downward trend was still observed. The results of this study are most clearly shown in Figures 7 and 8. For consistency, the constant flow rate of 18 m^3h^{-1} was maintained and the inlet temperature was varied from 10℃ to 80℃ during the simulations. The decrease in the reservoir temperature increases as the inlet temperature decreases. However, the decrease in the reservoir temperature does not have much effect on the outlet temperature. This is important for the coaxial DBHE system performance in terms of the stability of the outlet temperature and the reservoir temperature at the bottom-hole of the system.

As shown in Figure 7, the performance of both wells shows that, at the optimum flow rate of 18 m^3h^{-1}, the outlet temperature of 45 ℃ is optimal at the inlet temperature of 10 ℃, and a temperature gain ($T_0 - T_i$) of 35 ℃ is obtained for the 30-year of simulation period. A small gain of 2 ℃ is obtained when 80 ℃ of the inlet temperature is given to the system. Since the outlet temperatures are very stable over the 30-year production period, both wells would be good candidates for baseload thermal power generation. Under these operating conditions, as shown in Figure 8, a 26% decrease in the reservoir temperature was observed at the bottom of the well at the end of the simulation period.

The resulting thermal power for different inlet temperatures and flow rates is almost the same for both E GrSk 3/90 and Gt GrSk 4/05 wells, as shown in Figure 9. This is due to the fact that the main determinants of the thermal power are the flow rate and the outlet temperature. The resulting temperature depends on the origin of the reservoir temperature in the bottom hole. As shown in Figure 9, the lower the inlet temperature, the higher the energy yield, which is also influenced by the higher flow rate applied to the system. The relationship between inlet temperatures and flow rates versus reservoir temperature is evaluated quantitatively.

While the use of a district heating source could be an option for this well, further study could be done to optimize the combination of operating parameters with the cyclic period to balance the heating and cooling demand. This should be done to achieve the maximum outlet temperature at the wellhead to meet the district heating demand. As in the simulation with the inlet temperature range of 10 ℃ to 80 ℃, the most achievable inlet temperature at the surface condition is 10 ℃ to 20 ℃. This considers the use of fresh water as the working fluid for the current simulated system. This would also be the subject of further study to determine the inlet temperature in relation to the heat source for the implementation of coaxial DBHE technology at the Groß Schönebeck site.

6. CONCLUSION

The numerical simulation of the coaxial DBHE at the Groß Schönebeck site shows that at a maximum bottom hole temperature of 138 ℃, an inlet temperature range of 10 ℃ to 20 ℃, and a maximum flow rate of 54.00 m^3h^{-1}, a maximum of 1000 kW thermal power can be achieved by each of the well E GrSk 3/90 and well Gt GrSk 4/05 (A2). The optimum combination of operating parameters is achieved when 10 ℃ inlet temperature and 18 m^3h^{-1} flow rate are applied to the system. With these operating parameters, a 30-year production life can be achieved with a maximum outlet temperature of 45℃ and a reservoir temperature drop of 37℃ at the bottom-hole of 3800 m TVD. These parameters result in a thermal power of approximately 700 kW.

REFERENCE

Balling, P., Maystrenko, Y., & Scheck-Wenderoth, M. (2013). The deep thermal field of the Glueckstadt Graben. *Environmental Earth Sciences*, *70*, 3505-3522.

Blöcher, M. G., Zimmermann, G., Moeck, I., Brandt, W., Hassanzadegan, A., & Magri, F. (2010). 3D numerical modeling of hydrothermal processes during the lifetime of a deep geothermal reservoir. *Geofluids*, *10*(3), 406-421.

Blöcher, G., Reinsch, T., Henninges, J., Milsch, H., Regenspurg, S., Kummerow, J., ... & Huenges, E. (2016). Hydraulic history and current state of the deep geothermal reservoir Groß Schönebeck. *Geothermics*, *63*, 27-43.

Christi, L. F., Sass, I., Norden, B., Blöcher, G., Zimmermann, G., & Hofmann, H. (2025). Repurposing of hydrocarbon wells for Enhanced Geothermal System (EGS) development. *Geothermics*, *128*, 103268.

Fromme, K., Michalzik, D., & Wirth, W. (2010). Das geothermische Potenzial von Salzstrukturen in Norddeutschland. *ZDGG*, *161*(3), 323-333.

Grunau, H. R. (1981). Worldwide review of seals for major accumulations of natural gas. *AAPG Bulletin*, *65*(5), 933-933.

Huenges, E. (2002). In-situ Geothermielabor Groß Schönebeck 2000/2001. *Scientific Technical Report/Geoforschungszentrum Potsdam*.

Huenges, E., Moeck, I., & Geothermal Project Group. (2007). Directional drilling and stimulation of a deep sedimentary geothermal reservoir. *Scientific Drilling*, *5*, 47-49.

IEA, 2022. Temperature in germany, 2000-2020. URL: https://www.iea.org/data-and statistics/charts/temperature-in-germany-2000-2020-2. accessed: 2024-08-16.

JINZhijun, L. (2006). A study on the distribution of saline- deposit in southern China. *Oil & Gas Geology*, *27*(5), 571-583.

Kaiser, B. O., Cacace, M., Scheck-Wenderoth, M., & Lewerenz, B. (2011). Characterization of main heat transport processes in the Northeast German Basin: Constraints from 3-D numerical models. *Geochemistry, Geophysics, Geosystems*, *12*(7).

Koltzer, N., Schoenherr, J., Sporleder, M., Niederau, J., & Wellmann, F. (2024). Repurposing idle wells in the North German Basin as deep borehole heat exchangers. *Geothermal Energy*, *12*(1), 35.

LBEG, 2021. Geothermische Nachnutzung von Bohrungen. Technical Report. Landesamt für Bergbau Energie und Geologie Niedersachsen (LBEG). Hannover, Germany. URL: https://www.google.com/url?sa=t&rct=j&q=&esrc=s&source=web&cd=&ved=2ahUKEwjfj8f9pPBAxU0hv0HHVEtA_wQFnoECAwQAQ&url=https%3A%2F%2Fwww.lbeg.niedersachsen.de%2Fdownload%2F115995%2FGeothermische_Nachnutzung_von_Bohrungen_2021_.pdf&usg=AOvVaw1B7482A3QXWQjE0kNEFNbp&opi=89978449.

Liu, W., Zhao, H., Liu, Q., Zhou, B., Zhang, D., Wang, J., ... & Wu, X. (2017). Significance of gypsum-salt rock series for marine hydrocarbon accumulation. *Petroleum Research*, *2*(3), 222-232.

Noack, V., Cherubini, Y., Scheck-Wenderoth, M., Lewerenz, B., Höding, T., Simon, A., & Moeck, I. (2010). Assessment of the present-day thermal field (NE German Basin) inferences from 3D modelling. *Geochemistry*, *70*, 47-62.

Norden, B., Förster, A., & Balling, N. (2008). Heat flow and lithospheric thermal regime in the Northeast German Basin. *Tectonophysics*, *460*(1-4), 215-229.

Norden, B., Förster, A., Behrends, K., Krause, K., Stecken, L., & Meyer, R. (2012). Geological 3-D model of the larger Altensalzwedel area, Germany, for temperature prognosis and reservoir simulation. *Environmental Earth Sciences*, *67*, 511-526.

Norden, B., Bauer, K., & Krawczyk, C. M. (2023). From pilot knowledge via integrated reservoir characterization to utilization perspectives of deep geothermal reservoirs: the 3D model of Groß Schönebeck (North German Basin). *Geothermal Energy*, *11*(1), 1.

Ramires, M. L., Nieto de Castro, C. A., Nagasaka, Y., Nagashima, A., Assael, M. J., & Wakeham, W. A. (1995). Standard reference data for the thermal conductivity of water. *Journal of Physical and Chemical Reference Data*, *24*(3), 1377-1382.

Regenspurg, S., Feldbusch, E., Byrne, J., Deon, F., Driba, D. L., Henninges, J., ... & Schubert, C. (2015). Mineral precipitation during production of geothermal fluid from a Permian Rotliegend reservoir. *Geothermics*, *54*, 122-135.

Regenspurg, S., Feldbusch, E., Norden, B., & Tichomirowa, M. (2016). Fluid-rock interactions in a geothermal Rotliegend/Permo-Carboniferous reservoir (north German Basin). *Applied Geochemistry*, *69*, 12-27.

Schmelzer, J. W., Zanotto, E. D., & Fokin, V. M. (2005). Pressure dependence of viscosity. *The Journal of chemical physics*, *122*(7).

Schneider, D., Brossmann, E., & Wetzel, H. (1997). Prenzlau geothermal heat exchanger-technical concept and performance; Erdwaermetiefensonde Prenzlau-technisches Konzept und Betriebserfahrungen.

Sippel, J., Fuchs, S., Cacace, M., Braatz, A., Kastner, O., Huenges, E., & Scheck-Wenderoth, M. (2013). Deep 3D thermal modelling for the city of Berlin (Germany). *Environmental Earth Sciences*, *70*, 3545-3566.

Younglove, B. A., & Ely, J. F. (1987). Thermophysical properties of fluids. II. Methane, ethane, propane, isobutane, and normal butane. *Journal of Physical and Chemical Reference Data*, *16*(4), 577-798.

Acknowledgement

This work is funded by the Interreg CENTRAL EUROPE Programmed with co-financing from the European Regional Development Fund through the TRANSGEO Project (CE0100071). The authors are grateful for the financial support of the Helmholtz Association's Initiative and Networking Fund for the Helmholtz Young Investigator Group ARES (contract number VH-NG-1516). We thank Computer Modelling Group Ltd. for providing their reservoir simulation suite for research purpose.